TWO-DIMENSIONAL NUMERICAL SIMULATION OF FLOWS OVER A VIRTUAL WAVY SURFACE

Diogo Costa Buarque
Instituto de Pesquisas Hidráulicas, Universidade Federal do Rio Grande do Sul
Av. Bento Gonçalves, 9500, CEP 90650-001, Porto Alegre - RS - Brasil
diogo.buarque@gmail.com

Edith Beatriz Camaño Schettini
Instituto de Pesquisas Hidráulicas, Universidade Federal do Rio Grande do Sul
Av. Bento Gonçalves, 9500, CEP 90650-001, Porto Alegre - RS - Brasil
bcamano@iph.ufrgs.br

Jorge Hugo Silvestrini
Departamento de Engenharia Mecânica, Pontifícia Universidade Católica do Rio Grande do Sul
Av. Ipiranga, 6681, CEP 90619-900, Porto Alegre - RS - Brasil
jorgehs@pucrs.br

Abstract
Flows over wavy surfaces are important for many engineering aplications and environmental problems. Understanding theirs behaviour is necessary to know the terrain effects on flow resistance, the mechanisms of bed motion and the sediment transport. The numerical simulations methods, particularly the Direct Numerical Simulation (DNS), are useful tools to describe the physical behaviour of the flow for different imposed conditions, providing details of its structure. In this work we carried out DNS of a two-dimensional incompressible flow over a wavy surface. The surface is represented by the Virtual Boundary Method and characterized by a sinusoidal function with amplitude $A = 1$ and wavelength $\lambda = 10 \cdot A$. A low-storage third-order Runge-Kutta Method is used for the temporal discretization of the governing equations and a sixth-order Compact Finite Differences schemes is applied for the spatial discretization. The incompressible condition is verified by solution of a Poisson equation for the pression. Periodic boundary conditions are adopted in streamwise direction, free-slip condition on top and no-slip condition at the wavy surface. Reynolds numbers 100 and 500, based on the amplitude and the mean streamwise velocity over the crest, are used. As preliminary results are shown the effects of the confinement on the flow in function of the height of the domain, the influence of the mesh resolution and the behaviour of the flow over the virtual wavy boundary.

Keywords: *Direct Numerical Simulation, Wavy Surfaces, Virtual Boundary Method*

1. Introduction

Flows over complex boundaries as hills and waves are of interest in a number of environmental and engineering problems, and there have many studies on this subject (Salvetti et al., 2001; Henn and Sykes, 1999; Pellegrini and Bodstein, 2004; De Angelis et al., 1997; Tseng and Ferziger, 2004; Belcher and Hunt, 1998). The wavy boundary exerts a net drag on flow over it and has significant effects on the mean flow and the turbulence statistics (De Angelis et al., 1997). These flows are subject to the effects of alternating convex and concave curvature and despite its geometrical configuration is fairly simple, the flows pattern is complicated.

Atmospheric flows are significantly accelerated over the top of hill and to know the height of the maximum wind speed-up is important in the estimation of wind energy to efficiently site the wind turbines and to calculate the wind loads on structures on hill tops. The flow over wavy surface, particularly over hills, increases the drag of the surface on the large scale atmospheric motion and this effect has to be known and introduced into numerical weather prediction in order to led to an important improvement on forecast (Salvetti et al., 2001; Belcher and Hunt, 1998). Rivers may have periodic irregularity well-known as *bed forms* and the sediments motion over these rivers bed depends on the mechanic structure of the flow. There are different kinds of bed forms and many of them can be treated as waves or hills. The study of the behaviour of the flow over bed forms is necessary to know its effects on flow resistance and to understand the mechanisms of bed motion and of the sediment transport. So, the study of these flows contributes to our fundamental understanding of mechanisms that control distorted flow and helps to answer practical environmental and engineering questions as the cited above.

The numerical simulation methods, particularly the Direct Numerical Simulation (DNS), are useful tools to describe the physical behaviour of the flow for different imposed conditions being used as complement of experimental and analytical researches (Moin and Mahesh, 1998). DNS can acurrated resolve all spatial and temporal scales present in the flow, providing details of flows structure that are often difficult to measure and offering controlled conditions in which certain aspects of the experimental set up can be varied rapidly. Nonetheless its application is at present limited to flows at low and moderate Reynolds numbers due the existent computational resources.

In numerical simulations of complex flows, one of the primary issues is the ability to handle with complex geometries. The use of a Cartesian scheme, where the governing equations are discretized on a regular grid not adjusted to the shape of the body, simplifies the grid generation but may not allow to adjust the grid on the body contour, nor to impose the boundary condition exactly at the wall. With the use of the Virtual Boundary Method the obstacle can be represented in a Cartesian mesh with the aid of an external force field added in the momentum equation. This method can be applicable to complex geometries while requiring significantly less computation than competing methods without loss of accuracy. Another advantage is that the re-mesh to accommodate changes in geometry is not necessary, since the force term is independent of the mesh grid.

This work represents the first stage of a numerical simulation of a two-dimensional flow over a virtual wavy boundary using DNS. Numerical simulations with Reynolds numbers 100 and 500, based on the amplitude and the mean streamwise velocity over the crest, are used. The purpose of this stage is to examine the effects of the confinement on the flow field in function of the height of the domain, the influence of the mesh resolution and the behaviour of the flow for different forms of application of the forcing term. These informations will serve as the basis for further investigation of the flow field over the wavy surface at different Reynolds numbers, wave amplitudes and wavelengths and for future examination of the variation of the flow field around dunes of different geometries in forthcoming papers.

2. Numerical Methodology

2.1 Governing equations

In order to model the flow of interest, we use the time-dependent incompressible Navier-Stokes equations

$$\frac{\partial \vec{u}}{\partial t} + \vec{\omega} \times \vec{u} = -\frac{\vec{\nabla}\Pi}{\rho} + \nu \nabla^2 \vec{u} + \vec{f}, \tag{1}$$

and the continuity equation

$$\vec{\nabla} \cdot \vec{u} = 0, \tag{2}$$

where t is the time, $\vec{u}(\vec{x},t)$ is the velocity field, $\vec{\omega}(\vec{x},t)$ is the vorticity field ($\vec{\omega} = \vec{\nabla} \times \vec{u}$), ρ is the density, ν is the kinematic viscosity, $\Pi(\vec{x},t)$ is the modified pressure field ($P + \frac{\rho u^2}{2}$) and $\vec{f}(\vec{x_s},t)$ is an external feedback force field applied in the boundary locations $\vec{x_s}(i_s, j_s)$ to model the presence of the obstacle.

2.2 Spatial Discretization

In order to provide an improved representation of the range scale present in the flow all the spatial derivatives of the governing equations are discretized using a sixth-order compact centred finite-differences scheme proposed by Lele (1992) and applied on a regular Cartesian grid.

The first and second order derivatives are approximated using

$$\alpha f'_{i-1} + f'_i + \alpha f'_{i+1} = a\frac{f_{i+1} - f_{i-1}}{2\Delta x} + b\frac{f_{i+2} - f_{i-2}}{4\Delta x}, \tag{3}$$

$$\alpha f''_{i-1} + f''_i + \alpha f''_{i+1} = a\frac{f_{i+1} - 2f_1 + f_{i-1}}{\Delta x^2} + b\frac{f_{i+2} - 2f_1 + f_{i-2}}{4\Delta x^2}, \tag{4}$$

where the sixth-order space accuracy is obtained with the parameters shown in Tab. 1.

Table 1. Parameters α, a and b to obtain the sixth-order space accuracy

equation	α	a	b
3	$1/3$	$14/9$	$1/9$
4	$2/11$	$12/11$	$3/11$

2.3 Virtual Boundary Method

To represent the presence of the immersed boundary in the Cartesian grid, we used the Immersed Boundary Method proposed by Goldstein et al. (1993), where the no-slip condition is imposed with the aid of an external force field added in the momentum equation.

The method proposed by Goldstein et al. (1993) is an explicit feedback forcing method and the forcing term takes the expression

$$\vec{f}(\vec{x}_s,t) = \varepsilon_s \left(\alpha \int_0^t \vec{u}(\vec{x}_s,t')dt' + \beta \vec{u}(\vec{x}_s,t') \right), \tag{5}$$

where t is the time, α and β are negative constants having dimensions T^{-2} and T^{-1}, respectively and $\vec{x_s}(i_s, j_s)$ is the boundary locations. The constant α is used to calibrate the oscillation frequency of the residual forced flow in the body, whereas β drives the damping process. ε_s is a Gaussian distribution used in order to generate a *smooth* surface than a step-like surface created by the application of the forcing term only to the grid sites of the rectangular grid where the no-slip condition is required. So, at each surface point x_s the force is defined by the Gaussian distribution

$$\varepsilon_s = e^{-\sigma r^2(x)}, \tag{6}$$

where σ is a constant used to adjust the smoothing and $r(x)$ is the vertical distance from the wavy surface to each adjacent grid node.

The obstacle represented in this work is a wavy surface defined by a sinusoidal function with amplitude $A = 1$ and wavelength $\lambda = 10 \cdot A$. A constant ε^* has been adopted to limit the Gaussian influence and to create a region where the no-slip condition is expected. The exact smoothing function is not crucial if sufficient spatial resolution has been used (Goldstein et al., 1993). In the current work the time integral of the forcing term is approximated as a Riemann sum. Figure 1 shows a sketch of a immersed wavy surface discretized by a Cartesian grid and its virtual representation.

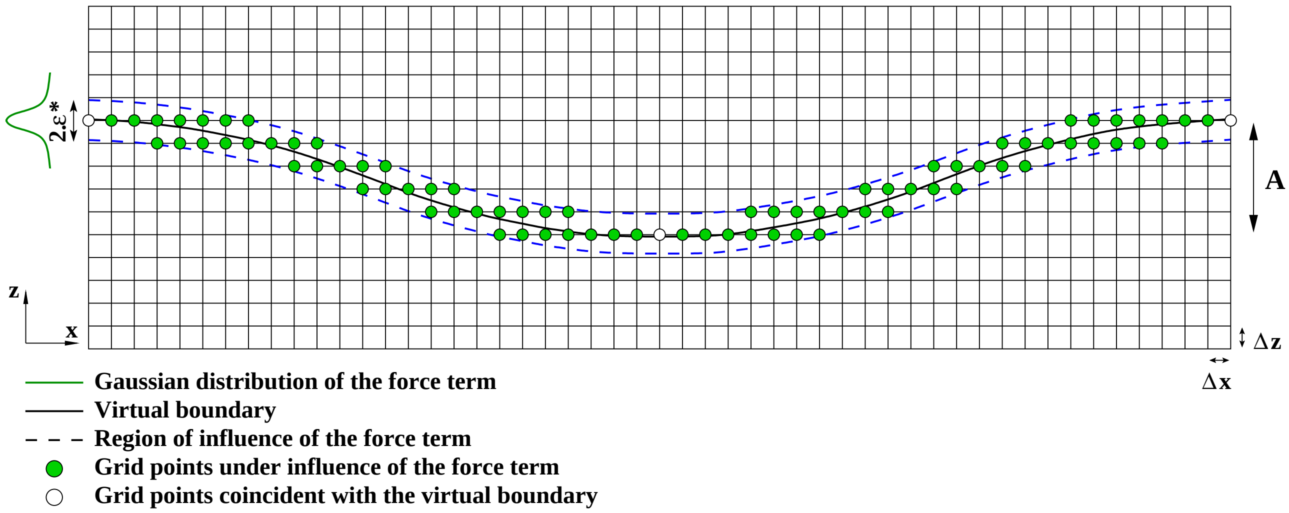

Figure 1. Virtual wavy surface and the computational Cartesian grid.

The time marching of the forcing term is done with a low-storage third-order Runge-Kutta scheme. The stability limit for the time step is given by

$$\Delta t < \Delta t_V = \frac{-\beta - \sqrt{(\beta^2 - 2\alpha k)}}{\alpha}\sqrt{3} \tag{7}$$

where k is a problem dependent constant of order one, Δt is the time step of the Runge-Kutta scheme and Δt_V is the time step of the virtual boundary method.

2.4 Temporal Discretization

In this study, the time integration is performed with three sub-time step applying the low-storage third-order Runge-Kutta method proposed by Williamson (1980). Considering the function $\vec{F}(\vec{u}) = \vec{f} + \nu\nabla^2\vec{u} - \vec{\omega} \times \vec{u}$, the time integration of the Eq. (1) from t_n to t_{n+1} gives

$$\frac{\vec{u}^{n+1} - \vec{u}^n}{\Delta t} = \frac{1}{\Delta t}\int_{t_n}^{t_{n+1}} \vec{F}(\vec{u})dt - \frac{\vec{\nabla}\Pi^{n+1}}{\rho}. \tag{8}$$

Since the numerical evaluation of the integral present in the force term is approximated as a Riemann sum performed at each sub-time step, the Eq. (8) can be split into two steps

$$\frac{\vec{u}^* - \vec{u}^n}{\Delta t} = \frac{1}{\Delta t}\int_{t_n}^{t_{n+1}} \vec{F}(\vec{u})dt, \tag{9}$$

$$\frac{\vec{u}^{n+1}-\vec{u}^{*}}{\Delta t}=-\frac{\vec{\nabla}\Pi^{n+1}}{\rho}, \qquad (10)$$

where $\frac{1}{\Delta t}\int_{t_n}^{t_{n+1}}\vec{F}(\vec{u})dt=\alpha_p\vec{F}(\vec{u}_{p-1})+\beta_p\vec{F}(\vec{u}_{p-2})$ and for $p=1,2,3$ we have $\vec{u}_0=\vec{u}^n$ and $\vec{u}_3=\vec{u}^*$.

The incompressibility condition is ensured with this fractional step method via resolution of a Poisson equation for the pressure.

Lele (1992) have shown that the stability limit for the Runge-Kutta scheme used is given by the CFL condition (*Courant-Friedrichs-Lewy*), which define the maximum time-step

$$\Delta t=\frac{\sqrt{3}\Delta x}{1,989\cdot U_\infty}, \qquad (11)$$

where U_∞ is the free-stream velocity.

3. Simulation Results

We use DNS to simulate two-dimensional flow over wavy surface channel. The governing equations are nondimensionalized using the mean streamwise velocity over the crest $(U_c=1)$ and the amplitude $(A=1)$. In all simulation are adopted periodic boundary conditions in streamwise direction, free-slip on top and no-slip at the wavy surface. As initial condition we use an uniform profile with $\vec{u}(x,z)=1$ for three simulations presented in this paper and a parabolic profile for the others. Both initial condition yield Reynolds numbers of about 100 and 500, based on A and U_c. The parameters of the simulations are shown in Tab. 2

Table 2. Parameters of the simulations

Simulation number	Initial condition	R_e	Domain $(L_x\times L_z)/A$	Grid	α	β	Virtual boundary
I	Parabolic	100	10×10	120×121	-260	-45	TS
II	Parabolic	100	10×10	120×121	-4080	-5	TS
III	Parabolic	100	10×10	120×121	-1690	-30	TS
IV	Parabolic	100	10×10	120×121	-260	-30	TS
V	Parabolic	100	10×10	120×121	-260	-15	TS
VI	Parabolic	100	10×10	120×121	-1040	-90	TS
VII	Parabolic	100	10×10	120×241	-1040	-90	TS
VIII	Parabolic	100	10×10	120×361	-1040	-90	TS
IX	Parabolic	100	10×10	240×241	-1040	-90	TS
X	Parabolic	100	10×10	240×361	-1040	-90	TS
XI	Uniform	100	10×10	120×241	-1040	-90	TS
XII	Uniform	100	10×12.5	120×301	-1040	-90	TS
XIII	Parabolic	500	10×10	180×361	-10000	-100	SS
XIV	Parabolic	500	10×10	180×361	-10000	-100	SC
XV	Parabolic	500	10×10	180×361	-10000	-100	TS

3.1 Application of the Force Field

The force field was applied in three different ways (simulations $XIII$, XIV and XV). Simulation $XIII$ was conducted to investigate the effect of a solid body on flow field. Hence, the forcing term was imposed using a Gaussian distribution only to the grid nodes located into a region limited by $\varepsilon^*=1.1\cdot\Delta z$, where Δz is the vertical mesh spacing, above the surface (*virtual boundary named SS*), while the grid nodes located *inside* of the boundary of the surface receive the whole forcing effect ($\varepsilon_s=1$). In this case, spatial oscillation in the normal and streamwise directions develops in the flow field when the feedback forcing function is applied, generating a discontinuity in the vertical profiles of streamwise velocity (Fig. 3) and an unrealistic perturbations in the immediate vicinity of the surface, as shown in Fig. (2a).

Simulation XIV differs from the previous one by a circulation region with vertical thickness ($10\cdot\Delta z$) just under the surface where no force is applied and a unphysical flow field is numerically allowed to develop inside (*virtual boundary named SC*). This internal flow field operated as a smoothing device allowing to eliminate the unrealistic perturbations in the immediate vicinity of the surface and to transfer them to the bottom of the circulating region (Fig. 2b), which is out of interesting flow field. The recirculation zone that appears in the trough due the separating flow downstream of the crest also contributes to this end and, what is more important, attenuates the discontinuity of the vertical profiles of streamwise velocity in the trough (Fig. 3).

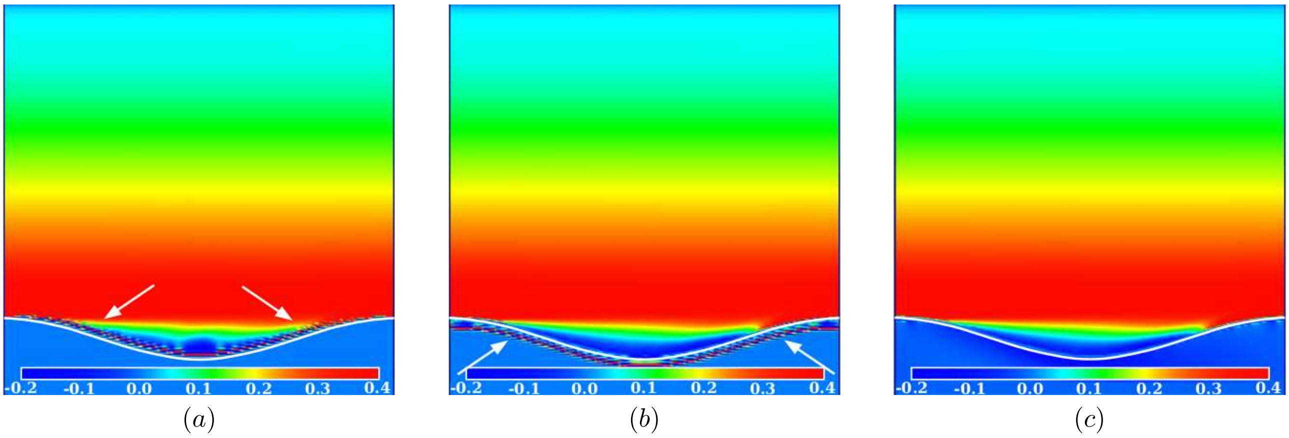

Figure 2. Re = 500, t = 237: Vorticity field. (a) solid surface – *SS*; (b) surface with circulation region – *SC*; (c) thin surface – *TS*.

In simulation XV the Gaussian distribution is used in order to apply the forcing term only into a region limited by the ε^* under and above the surface (*virtual boundary named TS*), as sketched in Fig. (1). In this case all unrealistic perturbations in the immediate vicinity of the surface can be eliminated (Fig. 2c) and the vertical profiles of streamwise velocity have a similar behaviour as in simulation XIV. The results of this simulation clearly allow to obtain the best results with a lower perturbation on flow field in comparison with the others. Furthermore, the time distribution of the l_2-norm error of velocities gets the lowest values, showing that the no-slip condition imposed is best attained for this case. Due this results, in all others simulations conducted here, the thin surface (TS) is adopted.

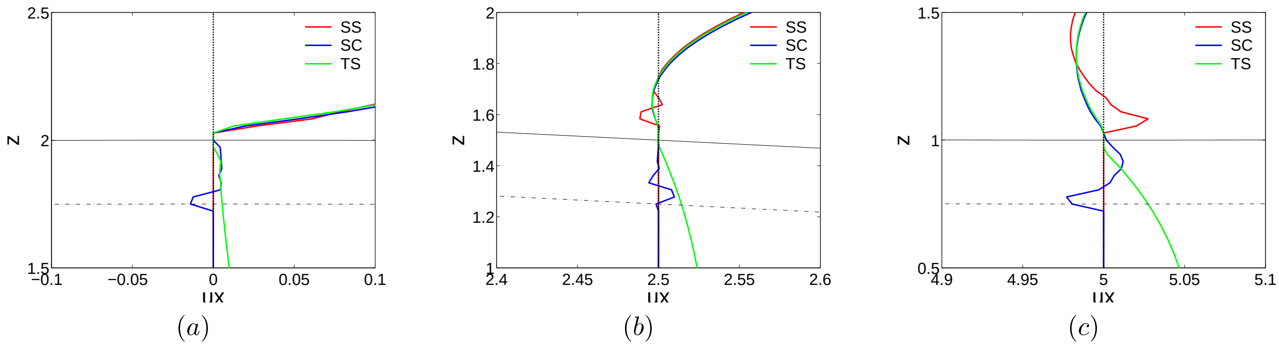

Figure 3. Re = 500, t = 237: Closeup at the vicinity of the wavy surface for the vertical profiles of streamwise velocity. (a) x = 0; (b) x = 2.5; (c) x = 5. The region between the solid and dash-dot black lines is the circulation region.

3.2 Virtual Boundary Method Parameters

The Virtual Boundary Method adopted has three parameters that must be defined: α, β and ε^*. This last one was fixed on as $\varepsilon^* = 1.1 \cdot \Delta z$ in order to apply the force term at least on three points where the mesh grid and the surface are coincidental. In order to define the other two parameters we carried out the simulations from I to V. Equation (7) shows that the constants α and β are important to determine the time step of the simulation. Decreasing α and increasing β makes the numerical solution more robust and larger time steps are possible (Von Terzi et al., 2001). If $\beta \to -\infty$ the time response of the feedback forcing tends to zero (Lamballais and Silvestrini, 2002) and the no-slip boundary condition is quickly attained.

The use of an explicit scheme for the time integration of forcing term presents a drawback for numerical stability reasons. The constrain (7) can be more severe than the CFL condition when very large values of α and/or β are used. According to Lamballais and Silvestrini (2002), the best forcing treatment can be conditioned by the temporal advancement of the forcing and viscous terms. Since the feedback forcing is explicitly integrated in time using the same scheme as for the convective and diffusive terms, in this work the choice of the time step is only restricted by the CFL condition, except for simulation VI. This choice imposes the use of moderate values of the couples α and β, which leads to residual velocities inside the boundary.

For each combination of α and β a different forcing function is added to the right-hand side of the Navier-Stokes equations, therefore a set of similar but slightly different response in reinforcing the no-slip condition is obtained for each of the solution. Also, for each time step limited by Eq. (11), is possible achieve pairs (α, β) that satisfy the stability limit giving by Eq. (7), (Fig. 4). The values of these parameters in simulations from I to III was chosen in order to attain this limit and to have the difference between the time-steps as short as possible.

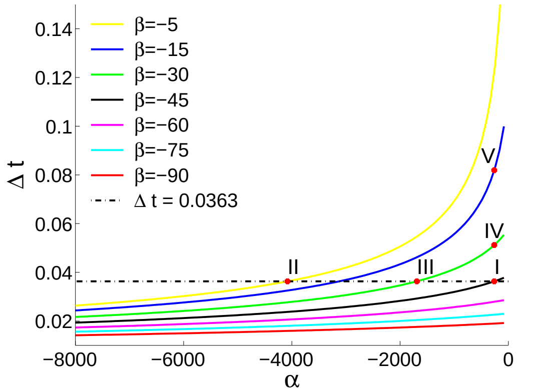

Figure 4. Δt in function of α and β. The strings from I to V refer to the simulations number in Tab. 3.

Table 3 shows the time steps of the simulations and the l_2-norm error of the streamwise velocity at the boundary points with respect to the no-slip boundary condition, which is defined as

$$l_2 - norm = \sqrt{\frac{1}{n_s}\sum_{i=1}^{n_s}(u(x_s,t))_i^2}, \tag{12}$$

where n_s is the number of virtual boundary points.

Table 3. Re = 100, t=3628.4: Simulations results for different values of α and β.

Simulation number	α	β	Δt Eq. (11)	Δt Eq. (7)	l_2-norm
I	-260	-45	0.036284	0.036293	$1.92 \cdot 10^{-6}$
II	-4080	-5	0.036284	0.036284	$1.12 \cdot 10^{-6}$
III	-1690	-30	0.036284	0.036303	$1.41 \cdot 10^{-6}$
IV	-260	-30	0.036284	0.051181	$1.47 \cdot 10^{-6}$
V	-260	-15	0.036284	0.081904	$1.20 \cdot 10^{-6}$

The simulations in Tab. 3 was conducted in order to examine the response of the virtual boundary to different pairs (α, β). These negative constants are determined by observing the response of the velocity field once the forcing term is applied. The effect of these parameters on l_2-norm and on the time evolution of the streamwise velocity is shown in Fig. (5).

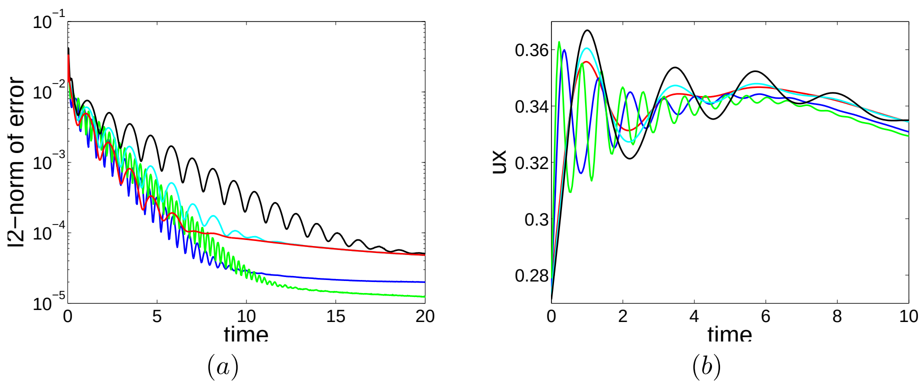

Figure 5. Re = 100. Effects of α and β parameters. Simulations I (red), II (green), III (blue), IV (cyan), V (black): (a) closeup at t = 20 of time distribution of the l_2-norm of error of the streamwise velocity; (b) closeup at t = 10 of vertical profiles of the streamwise velocity at (x=0, z=2.5).

As we can see in Fig. (5a), keeping up α as a constant and increasing β the time response of the virtual boundary decreases, but the magnitude of l_2-norm are practically the same. On the other hand, keeping up β as a constant and increasing α a lower magnitude of l_2-norm can be obtained and the oscillation frequency of the streamwise velocity decreases (Fig. 5b), but practically no substantial effect is observed on time response.

Using pairs (α, β) where $\Delta t < \Delta t_V$ and the difference between them is as short as possible, like in simulations I, II and III, Fig. (5b) shows that a lower oscillation at the streamwise velocity is obtained for the higher value of β. So, these test cases suggest that higher values of the coefficients allow the method to respond faster to any unsteadiness in the flow field and act more efficiently in reinforcing the no-slip condition. Nonetheless, no substantial difference was founded on flow field away from the boundary surface.

3.3 Mesh Resolution

In order to analyze the effects of mesh resolution in flow field we carried out simulations from VII to X. The time evolution at the position $(x, z) = (0, 2.5)$ and the l_2-norm of error of the streamwise velocity are shown in Fig. (6).

As we expected, the mesh resolution significantly affects the flow field since more large range of scales can be resolved as much refined the mesh is. Despite the use of the Gaussian in order to blur the location of the boundary and to generate a smooth surface, a step-like surface still appears for a mesh of about 120×121 due to this poor mesh resolution.

Fig. (6a) clearly indicates that the streamwise resolution practically doesn't affect the virtual boundary representation and the flow field. This observation indicates that the computational cost can be significantly reduced if a lower mesh resolution is adopted in this direction than the vertical direction.

As we can see in Fig. (6b), the l_2-norm of the streamwise velocity is of the same order for all the simulations, what indicates that the no-slip boundary condition is not affected by the mesh resolution.

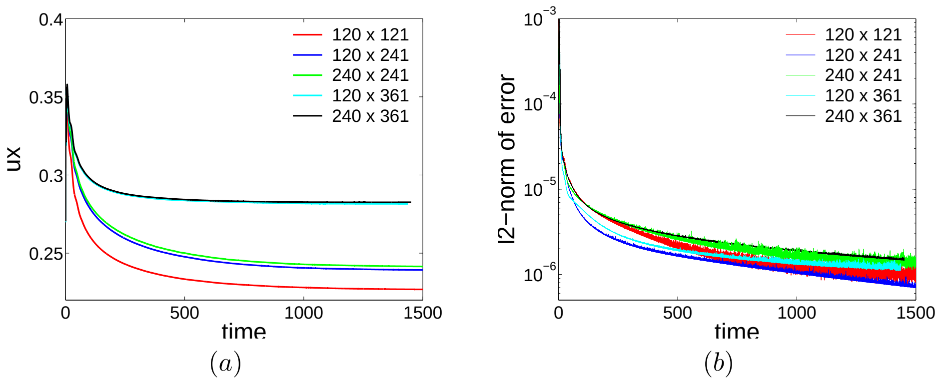

Figure 6. Re = 100. Effects of mesh resolution on streamwise velocity: (a) time evolution at x = 0 and z = 2.5; (b) time evolution of l_2-norm of error.

3.4 Confinement Effects

In order to verify the effects of different domains height on flow field we carried out the simulations VI and VII. The mesh resolution is the same in both cases and was chosen in function of the computational cost. The initial condition used was the uniform profile, which allows a best control of the mean flow, in comparison with the parabolic profile. The disadvantage of this initial condition is the long time necessary to reach a steady state and the initial perturbation generated on the mean flow, principally close to the surface.

Figure (7a) shows the vertical profiles of streamwise velocity at different location along the wavy surface for $t = 2286$. This figure clearly indicates that decreasing the domain height the streamwise velocity is accelerated far away from the surface.

The flow over the wavy surface separates just downstream of the crest and an recirculation zone appears. In the re-attachment region, just downstream of the trough, a thin accelerating boundary layer forms due to the decreasing cross-section and lifts away from the surface forming a detached shear layer as it moves over the crest. As shown in Fig. (7b and 7c), the domain height affects this acceleration, which increases with a decreasing height. The detached shear layer is also affected by the domain height and a reduction on the vorticity field over the crest is observed for the higher domain.

With respect of the l_2-norm of error of the velocities, the height of the domain does not affect its values. This observation shows that the response of the virtual boundary in reinforcing the no-slip condition is not affected by the domain height.

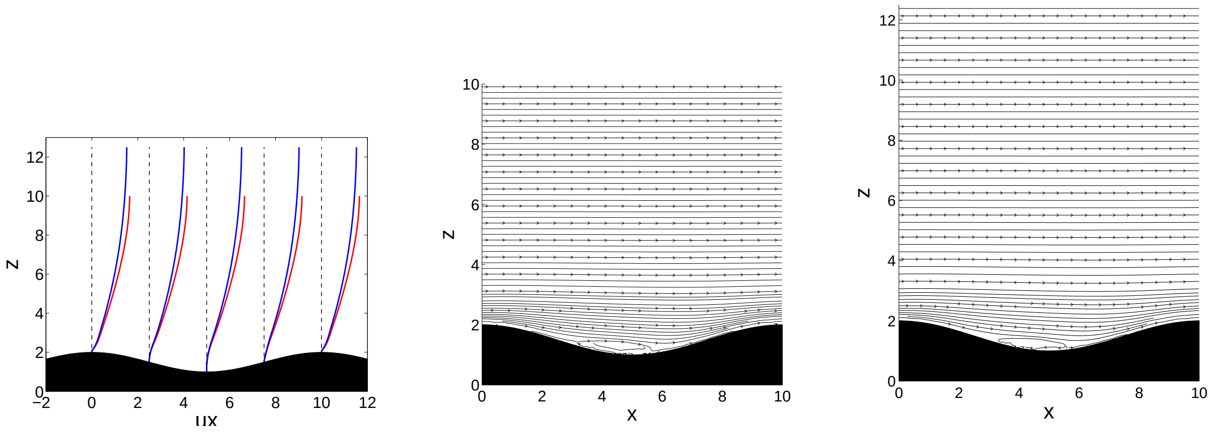

(a) (b) (c)

Figure 7. Re = 100, t = 2286: Simulations with different domain height: (a) vertical profiles of streamwise velocity at x = 0, 2.5, 5, 7.5 and 10, Lz = 10 (red), Lz = 12.5, (blue); (b) streamline for Lz = 10; (c) streamline for Lz = 12.5.

4. Conclusions

In this study, DNS of two-dimensional flow over a virtual wavy surface was conducted as a first stage for investigating the behaviour of this flow. The application of the virtual boundary method to represent a solid surface induced unrealistic perturbation close to the surface, which was drastically reduced with the application of the forcing term only at grid points which define the boundary. The surface ondulation induces alternating occurrence of favorable and adverse pressure gradients, periodic changes of the streamline curvature and a recirculating flow region appears near the trough of the wall. This recirculating region allows to attenuate the discontinuity in the vertical profile of streamwise velocity that appears exactly at the surface due the forcing field. When the restriction of the time-step is conditioned by CFL condition, the use of moderates values of constants α and β is imposed and hence residual velocities at the boundary surface are maintained, but its is considered to be weak enough to mimic realistically the no-slip condition. The domain height affects the flow field reducing the vorticity over the crest and accelerating the flow at the top of the channel for large height. The predicted results will be used for the continuity of this work allowing a further investigation of the flow field over different wavy surfaces and future examination of the behaviour of flows over bed-forms well-known as dunes.

5. References

Belcher, S. E. and Hunt, J. C. R., 1998, Turbulent flow over hills and waves, “Annu. Rev. Fluid Mech.”, Vol. **30**, pp. 507–538.

De Angelis, V., Lombardi, P., and Banerjee, 1997, Direct numerical simulation of turbulent flow over a wavy wall, “Phys. Fluids”, Vol. **9(8)**, pp. 2429–2442.

Goldstein, D., Handler, R., and Sirovich, L., 1993, Modeling a no-slip flow boundary with an external force field, “J. Comp. Phys.”, Vol. **105**, pp. 354–366.

Henn, D. S. and Sykes, R. I., 1999, Large-eddy simulation of flow over wavy surfaces, “J. Fluid Mech.”, Vol. **383**, pp. 75–112.

Lamballais, E. and Silvestrini, J. H., 2002, Direct numerical simulation of interaction between a mixing layer and a wake around a cylinder, “J. Turbulence”, Vol. **3(28)**, pp. 1–21.

Lele, S., 1992, Compact Finite Difference Schemes with Spectral-like Resolution, “J. Comp. Phys.”, Vol. **103**, pp. 16–42.

Moin, P. and Mahesh, M., 1998, Direct numerical simulation: a tool in turbulence research, “Annu. Rev. Fluid Mech.”, Vol. **30**, pp. 539–578.

Pellegrini, C. C. and Bodstein, G. C. R., 2004, The height of maximum speed-up in the atmospheric boundary layer flow over low hills, “J. of the Braz. Soc. of Mech. Sci. and Eng.”, Vol. **XXVI (3)**, pp. 249–259.

Salvetti, M. V., Damiani, R., and Beux, F., 2001, Three-dimensional coarse large-eddy simulation of the flow above two-dimensional sinusoidal waves, “Int. J. Numer. Methods Fluids”, Vol. **35**, pp. 617–642.

Tseng, Y. H. and Ferziger, J. H., 2004, Large-eddy simulations of turbulent wave boundary flow - ilustration of vortex dynamics, “J. Turbulence”, Vol. **5 (34)**, pp. 1–23.

Von Terzi, D. A., Linnick, M. N., Seidel, J., and Fasel, H. F., 2001, Immersed boundary techniques for high-order finite-difference methods, “AIAA Paper”, Vol. **1 2918**, pp. 17p.

Williamson, J. H., 1980, Low-Storage Runge-Kutta Schemes, “J. Comp. Phys.”, Vol. **35**, pp. 48–56.